Wetting of Fiber Mats for Composites Manufacturing: I. Visualization Experiments

Yung-Tin Chen, H. Ted Davis, and Christopher W. Macosko
Dept. of Chemical Engineering and Materials Science, Center of Interfacial Engineering, University of Minnesota, Minneapolis, MN 55455

Wetting of glass fibers was visualized using an oil with the same refractive index. With both a video-enhanced microscope and a high-magnification video camera we followed the flow front and qualitatively measured the entrapped air bubbles by image analysis. Due to different permeabilities between the fiber mats and bundles, air bubbles are entrapped. Two major kinds of air bubbles are observed: small cylindrical micro voids between fiber filaments (inside fiber bundles) and spherical macro voids outside fiber bundles. These air bubbles can be described by three major mechanisms: initial liquid bypassing/air trapping, later capillary invasion of disordered fiber bundles, and air bubble mobilization. Both random and unidirectional fiber mats were used in this study. Vacuum as well as different fluid viscosities and surface tensions were also investigated, which led us to guidelines of optimum processing parameters of fiber wetting for resin transfer molding and structural reaction injection molding. They are low viscosity, vacuum, high mold temperature, and high pressure.

Introduction

A major limitation of all high-speed composite processing is the wetting of fibers. The time it takes a resin to wet fiber tows controls both the quality of the products and the rate at which it can be produced in composite manufacturing. In resin transfer molding (RTM) or structural reaction injection molding (SRIM) processes, resins are forced to penetrate through fiber networks, driving out the air that is initially in the space between individual fibers. Incomplete wetting or impregnation often results in the formation of voids or air entrapment. Although the occurrence of voids has been frequently documented and is recognized as a major problem in composites (Bascom and Romans, 1968; Kohn et al., 1968; Williams et al., 1974; Judd and Wright, 1978; Gonzalez, 1983; Behrens, 1983; Macosko, 1989; Kardos et al., 1986; Kamal et al., 1986; Gutowski et al., 1987; Molnar et al., 1989; Elmendorp and During, 1990; Hayward and Harris, 1990; Parnas and Phelan, 1991; McGeehan, 1991; Mahale et al., 1992; Lundstrom et al., 1992; Stabler et al., 1992), the exact mechanism of void formation is not clear due to its complexity. Generally, the void or air bubble formation can include mechanical entrapment as well as growth of bubbles existing in the resin phase.

Bascom and Romans (1968) were the first to report that micro voids were trapped in the resin between individual fibers in glass–resin composites. They reported that the micro voids entrapped were 10^6 to 10^8 voids per cubic centimeter in filament winding process. They found that reducing the contact angle to zero, and causing the tension to oscillate as the strand passed through the resin, markedly reduced the number of voids. A quantitative measurement of void content in glass-filament-wound composites was carried out by Kohn et al. (1968). They measured void content by the statistical point-count method. Judd and Wright (1978) reported that the interlaminar shear strength decreased by about 7% for each 1% void detected. The voids remaining on the fiber surface can initiate fiber/matrix debonding upon cyclic loading of the composites.

Mahale et al. (1992) used the refractive index matching technique and image analysis to measure void formation during liquid impregnation of nonwoven multifilament glass fiber mats. They reported that void content was a function of the capillary number characterizing the flow process. From their work, there emerges a critical value of capillary number, Ca $= 2.5 \times 10^{-3}$, below which void content increased exponentially with decreasing capillary numbers. Above this critical

value, negligible entrapment of voids was observed. Their study implies that voids can be ignored at high flow rates or short mold filling time. This is obviously contradictory to the conventional experimental observations in resin transfer molding (Molnar et al., 1989). It seemed that Mahale et al. considered the air bubbles outside fiber bundles only.

Parnas and Phelan (1991) presented a model of mechanical trapping of air inside fiber bundles for flow perpendicular to the fibers. They took into account two competing flow processes that occur simultaneously in the fiber mats: the macroscopic flow of the resin through the preform (Figure 1b) and the impregnation of the individual fiber bundles that make up the preform (Figure 1a) Due to the flow into fiber tows, the model prediction leads to a higher value of the effective permeability than would be obtained in saturated preforms. Also their fiber impregnation model allowed for the estimation of void volume in the cured part. Chan and Morgan (1992) assumed the same two competing flow processes and proposed a model for flow parallel to the fiber axis. For the ideal case of void formation arising from pressure differences only, the model predicts void formation localized at the resin front region. But neither of these studies takes into account the role of surface tension in the penetration process. For example, the model cannot explain the fact that fewer voids result from slow filling processes.

In order to understand better the mechanisms of air entrapment during fiber impregnation, we design a novel optical isorefractive technique to visualize the dynamic fiber wetting process with a high-magnification video camera and a video-enhanced microscope. The goal of the study is to understand the mechanisms of air entrapment and to find the ways to improve wetting in polymer composite processing. The amount of air entrapped under different processing parameters such as velocity, viscosity, surface tension, fiber types, and fiber volume fraction was investigated. Simple models are proposed to explain air entrapment during RTM/SRIM processing in Part II. (Chen et al., 1995)

Wetting Visualization Experiments

A high-magnification video camera and a video-enhanced microscope were used for fiber-wetting visualization. The experimental setup of a high-magnification video camera is illustrated in Figure 2. The system included a rectangular transparent mold connected to a liquid transfer unit that drove an index matching liquid through the fiber prepacked mold. The mold's top and bottom components were made of polycarbonate plates. This allowed the back-lit fiber mat samples to be viewed during and after fluid injection. Two aluminum clamps were used to assemble the polycarbonate plates. The thickness of the mold was controlled by different aluminum spacers and gaskets. Silicon rubber gaskets were inserted between the polycarbonate plates and aluminum spacers in order to prevent leakage. A lamp with a strong uniform light (from Aristo Grid Lamp Co., New York) was used as the light source. The lamp was placed vertically below the polycarbonate mold. The assembled polycarbonate mold was connected to a nitrogen gas tank or a syringe pump. An immersion oil of 1.557 refractive index (from Cargill Labs. Inc., Cedargrove, NJ), which best matched the glass fibers, was used. When good oil-to-glass contact was made, bubbles showed up as black on a semitransparent background.

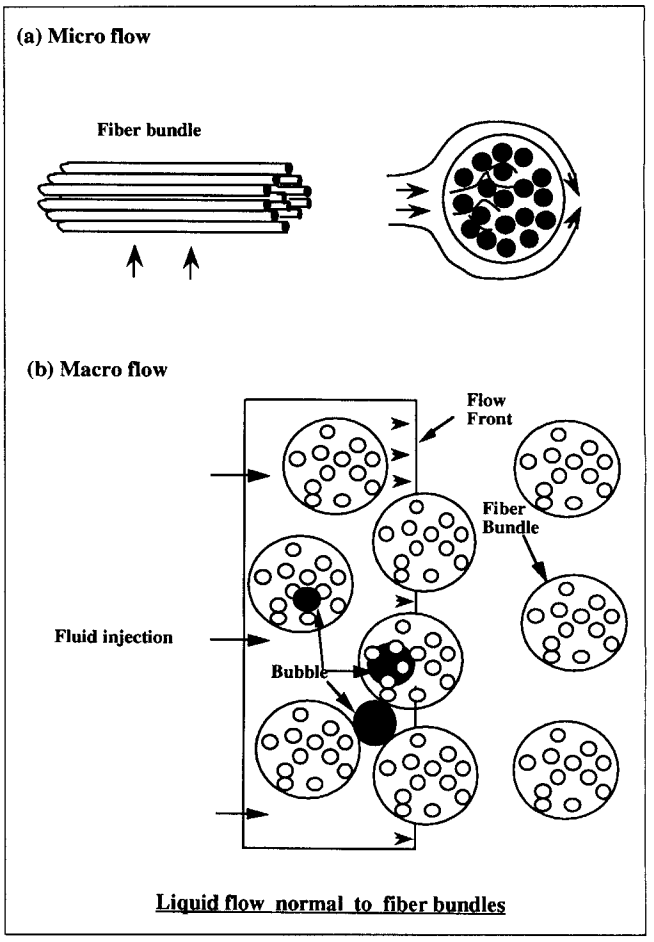

Figure 1. Two levels of impregnation in resin transfer molding process: (a) micro flow-bundle level; (b) macro flow-mat level.

The motion and flow front of the invading liquid were captured by a microscope camera placed vertically on top of the mold with a tripod. The magnification of the microscopic

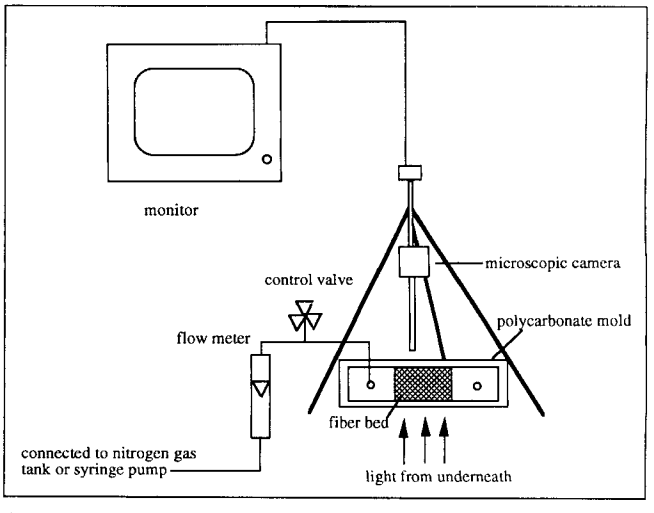

Figure 2. Experimental setup for fiber-wetting visualization.

Table 1. Properties of Fiber Mats Used

	Dia. (μm)	Porosity	Permeability (1×10^{-8} cm^2)
Random fiber mats		0.7–0.9	350–2,000
Fiber bundle	100–300	0.38	0.4 (axial)
			0.05 (transverse)
Unidirectional fiber mats		0.6–0.9	50–400
Fiber bundle	2,500–3,000	0.44	0.35 (axial)
			0.04 (transverse)

Table 2. Properties of Test Liquids Used

	σ (dyne/cm)	η (cp)	cos θ	n_D (25°C)
Pure immersion oil * (Cargill Lab.)	33.5	51.5	0.45	1.557*
Oil + surfactant † (H-Si 2311)	26.4	51.5	0.95	1.557†
Epoxy ‡ (Epon 815)	44.0	650	0.32	1.57‡

* From Cargill Labs. Inc., Cedargrove, NJ.
† From Goldschmidt Chemical Co., VA.
‡ From Shell Chemical Co., Houston, TX.

camera (range from 15× to 120×) could be varied by using different magnification lenses. The images of the flow visualization were recorded by a VCR.

The visualization experiment was controlled to make sure that no bubbles were introduced either in the injection liquid or in the injection line. It can be helpful to pull a vacuum on the oil to quickly remove any bubbles. Precaution should be taken so as not to pour the liquid quickly into any holding tanks, which can also create small bubbles in the liquid. The gaskets held up to 7×10^5 Pa. Leaks only occurred when the gaskets had been used many times. The gaskets tended to deform and slip out from between the mold pieces. If the gaskets were wiped clean between each use, they would not slip. For best results, the mold bolts were tightened up until the gasket just began to expand past the mold edges. The gasket expansion up to the edge of the fiber mat also prevents oil channeling around it.

Fibers and test liquids used

Two different fiber mats were tested in this study: continuous random fiber and unidirectional fiber mats. The continuous random fiber mats were obtained from Owens Corning Fiberglas (M8610); the unidirectional fiber mats were from CoFab (A1010). The fibers are sized with a silane coupling agent containing hydroxyl groups. A thermoplastic polyester

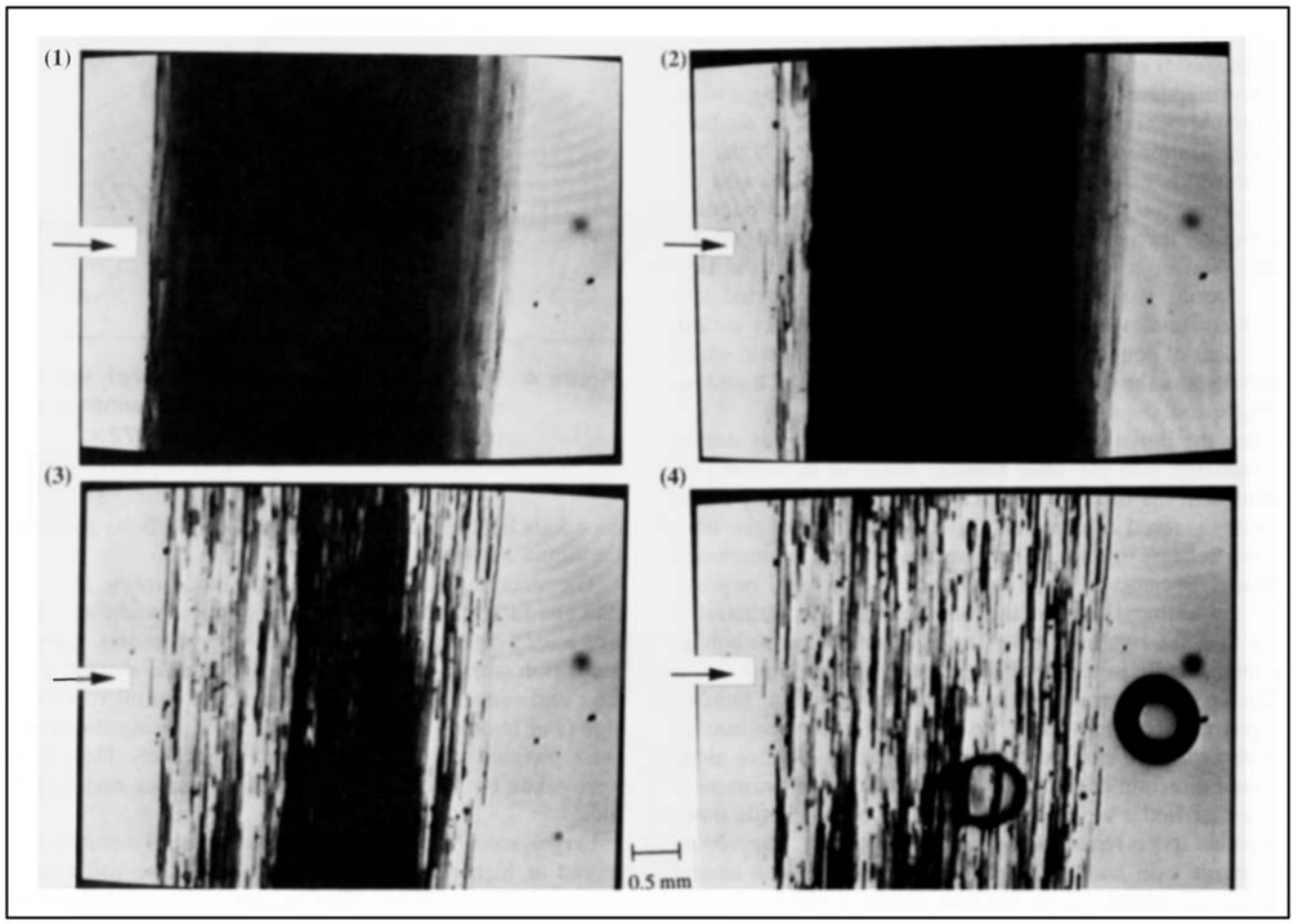

Figure 3. Transient flow front transverse to fiber bundles, velocity = 0.13 cm/s, porosity = 0.44.
(1) 0.00 s; (2) 0.59 s; (3) 4.29 s; (4) 11.78 s.

binder is applied to hold the strands together and permit handling of the mats. The fibers were used as received. The average fiber bundle diameters, porosities, and experimental permeabilities are listed in Table 1. The determination of these parameters can be found in Chen (1993).

The surface tension, viscosity, wetting contact angle, and refractive index of the test liquids used in this visualization experiment are listed in Table 2 [measured by standard techniques as discussed by Chen (1993)]. Immersion oils with and without surfactant were tested in order to investigate the effect of surface tension. Epoxy resin was also used to investigate the effect of viscosity.

Wetting Visualization Results

Void formation and mechanisms of air entrapment

A representative microscopic transient flow front perpendicular to a single fiber bundle at different contact times is shown in Figure 3. The first picture shows the dry fiber before fluid invasion. The other three pictures show the fiber at contact times of 0.59, 4.29, and 11.78 s, respectively, at a fluid-invading speed of 0.13 cm/s. The fluid-invading velocity was estimated by measuring the average superficial velocity through the whole mold. The zero contact time is defined as the first instant that the liquid touched the dry fiber bundle. By measuring the volume and weight of the sample, the porosity was estimated to be about 0.44.

These series of flow front images depicted three major steps of air entrapment: initial liquid–fiber contact and bypassing, then liquid penetration after bypassing, followed by air bubble mobilization. The initial contact and bypassing is the period in which liquids first contact the fiber bundles and bypass them through the larger passage between fiber bundles. The liquids then wrap around the fiber bundles and join together, leaving a large portion of dry fiber behind the flow front. During the bypassing the liquids also penetrated into the fiber bundles at the same time due to capillary action. The extent of penetration depends on the time scale in which liquids bypass the fiber bundles, in other words, the liquid-invading speed.

After the initial contact and bypassing, the liquids started to penetrate into the fiber bundles from all directions. As indicated in the third picture of Figure 3, the majority of the air was squeezed or compressed into the center of the fiber bundle because of liquid penetration as well as increased pressure. Because of the direction of initial liquid penetration, the lefthand side of the fiber bundle was penetrated more than the righthand side (the righthand side was behind the fiber bundle in terms of liquid invading direction).

During the penetration process, the entrapped air bubbles are still in a transient state. To balance the surface tension and viscous force exerted on them, they tend to move along the axial direction of the fiber bundles. During the movement they either find a larger pore and escape or they settle down at another pore space inside the fiber bundle. They could also merge with another void. If the surface tension cannot hold the air bubble, as in the case shown in the fourth picture of Figure 3, the inertial force or pressure gradient will force the air out of the fiber bundles. In this study, this process is referred to as the *mobilization mechanism*. The escaped air bubble has a spherical shape and flows along with the liquid between fiber bundles.

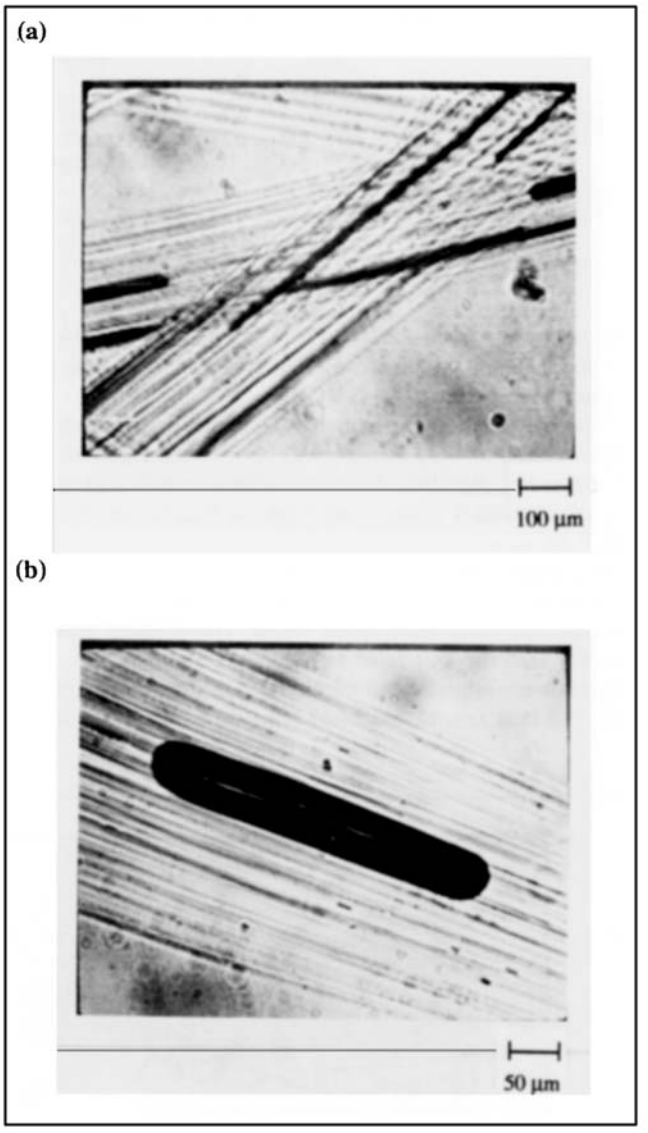

Figure 4. Representative cylindrical (micro) voids inside fiber bundles from video-enhanced microscopy (VEM): (a) 136×; (b) 272×.

The sizes and shapes of voids entrapped inside fiber bundles are different. The smaller ones or micro voids, are shaped like a long cigar squeezed between fiber cylinders. Close examination with a video-enhanced microscope showed a concave end surface. A representative picture of micro voids inside fiber bundles is shown in Figure 4. The magnifications of these pictures are 136× and 272×, respectively. Flow images were taken by VEM using the refractive index matching liquid.

Larger voids inside fiber bundles are also sometimes observed at higher liquid-invading speed. These voids are referred to as *meso voids*. They occupy a relatively larger area encompassing several fiber filaments. The cylindrical ends of these meso bubbles are distorted by the interferences of fiber filaments. The overall shapes look like a stack of several flat

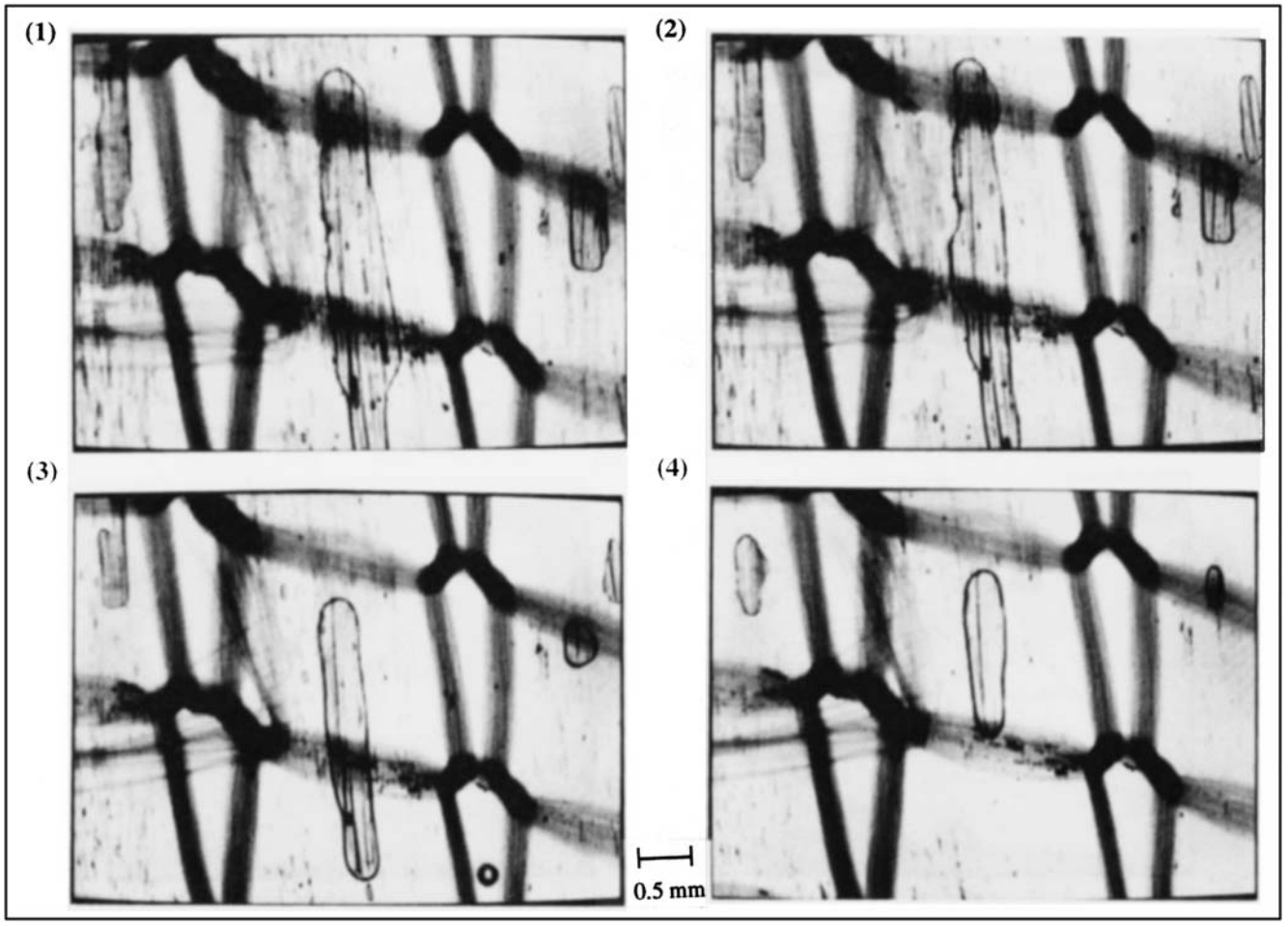

Figure 5. Shrinking of bubble size at different pressure drop, porosity = 0.86.

(1)ΔP = 5 psi (34 kPa); (2) ΔP = 15 psi (103 kPa); (3) ΔP = 40 psi (276 kPa); (4) ΔP = 70 psi (482 kPa).

sausages of different sizes (Figure 5). The meso voids are observed mostly on the surface of the composites due to the larger pore space between fiber mats and the mold surface.

During the liquid penetration, not only can the location and shape of air bubbles change, but the sizes can also vary with time due to the increasing pressure surrounding the fiber bundles. To illustrate the effect of increasing pressure on the size of air bubbles, an example is shown in Figure 5. These pictures show the shrinking of meso air bubbles that were subjected to a pressure drop at 5, 15, 40 and 70 psi (34, 103, 276 and 482 kPa), respectively. The initial bubble was formed at a pressure drop of 5 psi (34 kPa) with porosity of 0.86. Each image was recorded after equilibrium was reached at different pressure drops. Note that the liquid was flowing during the whole event. It is also important to notice that even at a much higher pressure drop (70 psi, 482 kPa) the air bubble was not pushed out of the fiber bundle. Higher pressure did not affect mobilization strongly in this case. This is because, owing to the high porosity of the fiber mat sample used, the pressure gradient inside the mold was relatively small.

Effect of liquid invading velocity on air entrapment

Flow Parallel to Unidirectional Fiber Bundle. Figure 6 shows the transient flow front parallel to a fiber bundle at a liquid-invading speed of 0.08 cm/s. This is the slowest invading speed among this set of experiments. The velocity was measured by taking the length of the fiber and dividing it by the time it took to pass the fiber. The time to pass the whole screen (which is equivalent to 0.5 cm fiber length) was taken by counting the number of frame laps in VCR slow-motion mode. The darker stripes seen in the picture were the nylon stitches that bind the fiber bundles together. The flow front, which is parabolic in shape, was pulled by the capillary force directed toward the dry fiber region on the righthand side. While the liquid passed over the fiber bundle, it penetrated down into the fiber bundle at the same time. Because the invading speed was slower than the capillary penetration speed, the air inside the fiber bundle had enough time to escape. This resulted in very little air entrapped. The small amount of air that was entrapped was mainly due to the unequal capillary velocity resulting from the unequal pore sizes inside the fiber bundle. The majority of the bubbles were small and had a long cylindrical shape.

The case of higher liquid invading speed is shown in Figure 7. At the invading speed of 0.86 cm/s, the liquid quickly passed through the spaces between fiber bundles due to their low resistance. The dry fiber was surrounded by the liquid

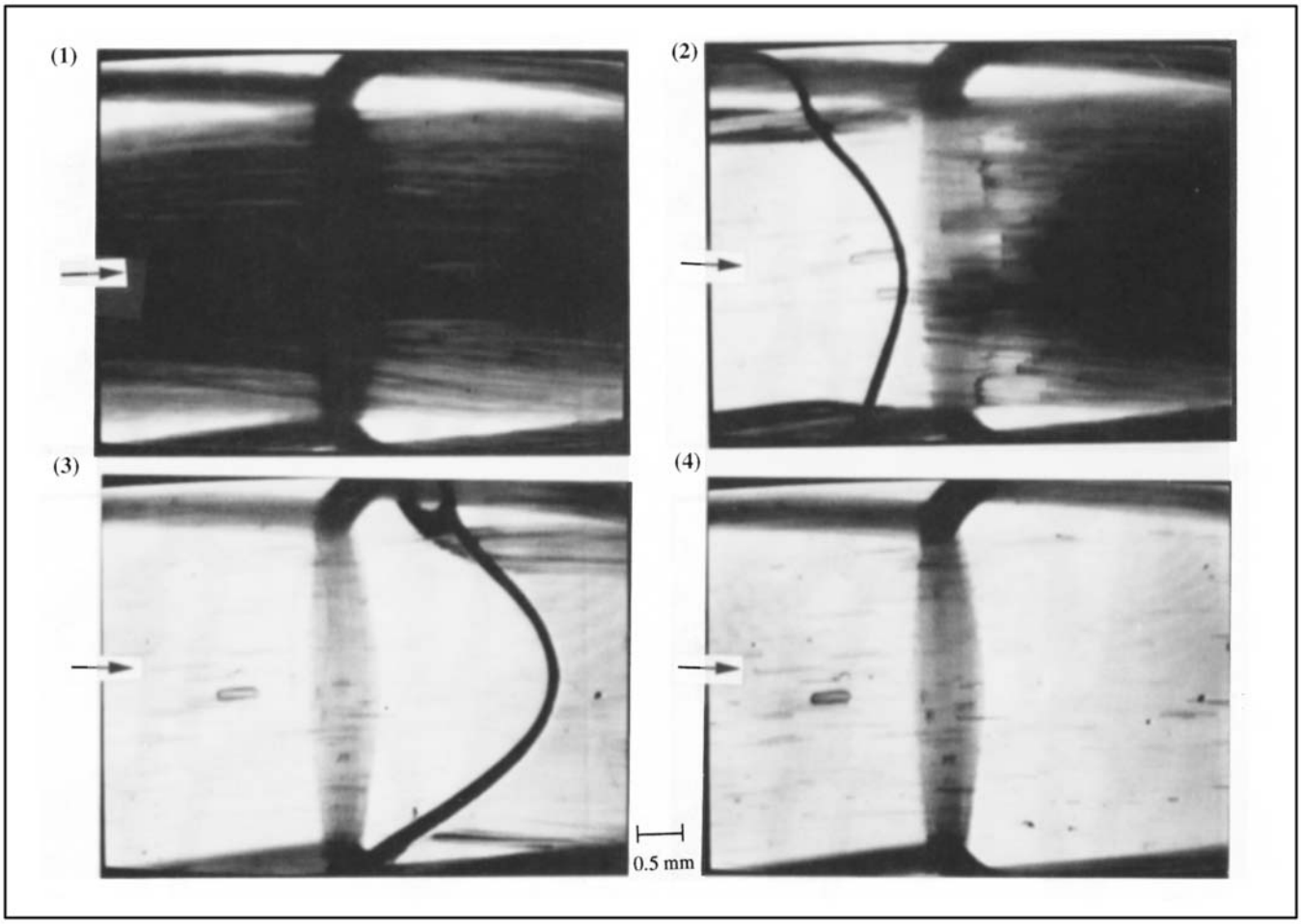

Figure 6. Transient flow front parallel to fiber bundles, velocity = 0.08 cm/s, porosity = 0.86.
(1) 0.00 s; (2) 2.3 s; (3) 4.7 s; (4) 5.8 s.

with the result that most of the air inside fiber bundles was trapped. Next, the liquid started to penetrate into the fiber bundle from the perimeter. In the second picture of this series, at a time of 0.95 s, the entrapped air is seen as a long dark region encompassing most of the dry fiber bundle. As the injection continued, the liquid kept penetrating into the fiber bundle, pushing away the air as shown in the third picture at a time equal to 2.5 s. The final status of the air entrapment is shown in the last picture of Figure 7 (at a time of 20.0 s). There remained a long meso void and numerous micro voids. Note that the location of the image shown in picture 4 was slightly shifted to the right from the previous picture in order to show the readers the whole meso void.

Flow perpendicular to unidirectional fiber bundle. The effect of liquid-invading velocity on bubble formation in flow transverse to the fiber direction was similar to that of flow in the parallel fiber direction. The quantity of air bubbles entrapped increased with increasing velocity of invading liquid. The bypassing of liquid and the initial trapping of air again played an important role. At a liquid-invading velocity of 0.14 cm/s, no meso void was observed. Whereas at a liquid-invading velocity of 1.21 cm/s, large amounts of meso voids were entrapped inside fiber bundles. The number of micro voids seemed to be less than in the case of slow liquid invasion due to a stronger mobilization effect.

Since the liquid-invading speed was greater than the capillary velocity, the liquid tended to first bypass the fiber bundles and then penetrate into them. The faster the invading speed, the less the initial penetration is. Above a certain invading speed, the degree of initial penetration could practically be neglected. The majority of penetration occurred after liquid bypassing. This penetration process is a complex pattern of the imbibition of liquid into a heterogeneous network of a porous medium. Here the porous medium is an array of nearly aligned cylindrical fibers, but whose fiber–fiber spacing varies from site to site. The penetration occurred not only across the fiber bundles but also in the axial direction of the fibers. Capillary penetration is much faster parallel than penetration transverse to the fiber direction. Thus at a slow liquid-invading speed the axial capillary penetration dominated.

During the penetration, the liquid is initially driven by surface tension, it then passes through small passages, overcomes surface tension at the neck, and continues to propagate to the next layer of fibers. Since the penetration speed at each pore throat is different, air will be entrapped in a larger pore space surrounded by a smaller pore throat by joining the micro flow fronts from other passages. The mechanism is further complicated by the fact that liquid also tends to move along the fiber axis. The combination of cross-fiber

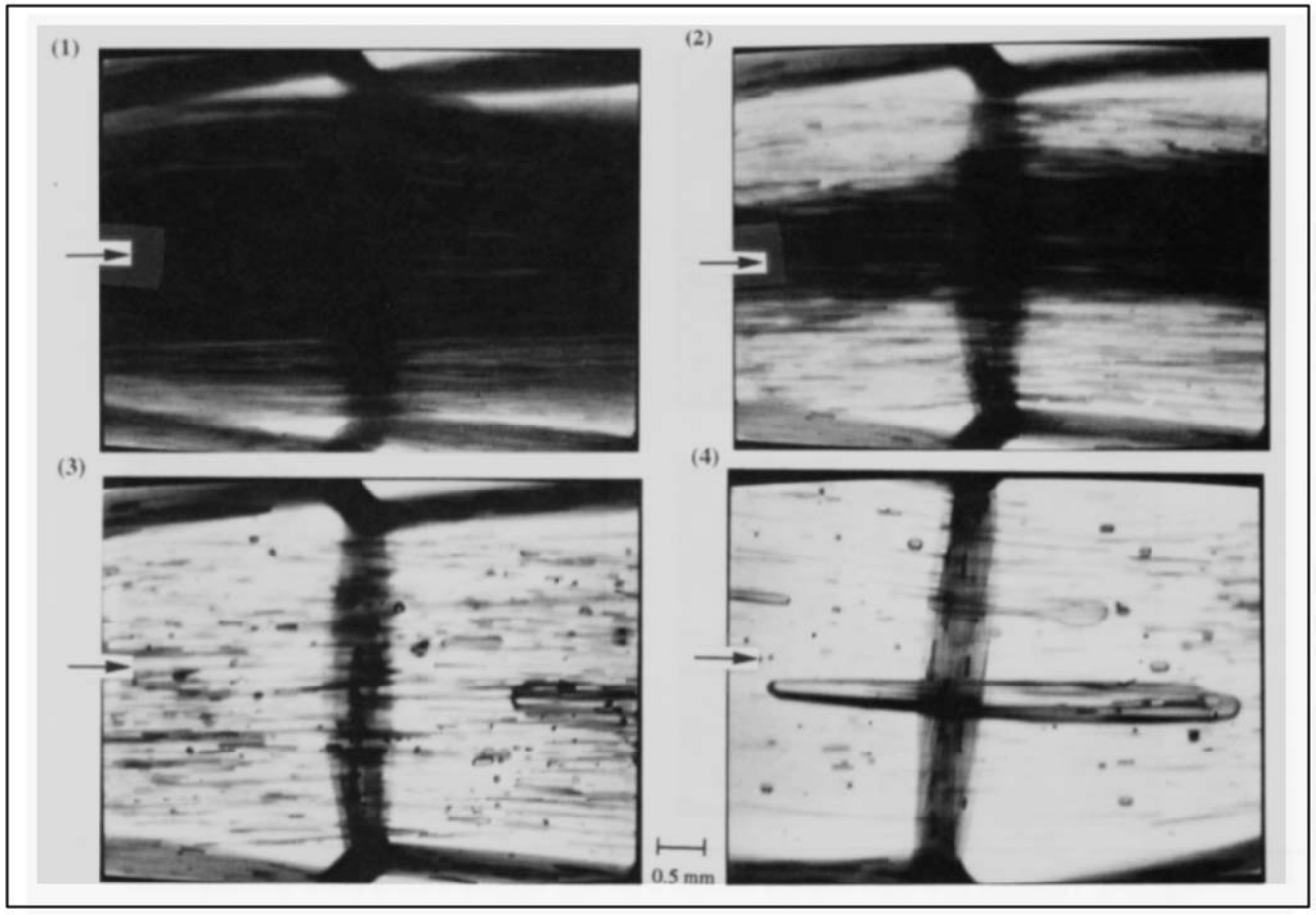

Figure 7. Transient flow front parallel to fiber bundles, velocity = 0.86 cm/s, porosity = 0.86.

(1) 0.00 s; (2) 0.95 s; (3) 2.5 s; (4) 20.0 s; another location, long rod bubble.

penetration and the movement along fiber axis is really a three-dimensional matter.

Flow Through Continuous Random Fiber Mats. Representa- visualization results of flow through continuous random fiber mats are shown in Figure 8 and Figure 9. The first one (Figure 8) shows the transient flow front of very slow liquid-invading speed, 0.078 cm/s at times of 4.36, 4.85, 8.34 and 9.2 s. The magnification is approximately 18×. At this slow speed, the capillary velocity along the fiber direction is faster than the macroscopic main flow velocity. Big voids are entrapped by the joining of the flow fronts along fiber bundles. The average diameter of these big air bubbles ranges from 500 to 1,000 μm. In the case of faster filling, as shown in Figure 9, large quantities of cylindrical micro voids were entrapped inside fiber bundles due to the bypassing of liquids outside fiber bundles. The velocity was 1.5 cm/s and the contact times were 0.07, 0.18, 0.23, and 0.3 s, respectively. The mechanisms of formation of these micro voids are the same as those of the unidirectional fiber bundles described earlier. Cylindrical micro voids entrapped inside the fiber bundles can be forced out when the viscous force is greater than the capillary force. These escaped spherical voids are large enough to be seen by the human eye and are conventionally the most undesirable ones.

Our observations on the effect of the liquid-invading velocity on the formation of air bubbles in random fiber mats can be summarized as follows: in the case of steady state, that is, if the liquid is pumped long enough, the number of spherical voids decreases with increasing velocity. If the liquid pumping is stopped at the end of mold filling instantly, the quantities of spherical voids seem to increase with increasing velocity. The preceding statement holds in the range where invading velocity is greater than a certain critical velocity. The critical velocity is the capillary velocity here. The results of our steady-state experiments are consistent with that obtained by Mahale et al. (1992). For the dynamic case, beyond a certain liquid invading velocity or pressure gradient, the air entrapped inside fiber bundles is forced out and forms spherical bubbles floating between fiber bundles, thus resulting in the increase of spherical bubbles. These bubbles eventually accumulate at the end of the fiber mold. This dynamic void trapping and mobilization is similar to what has been observed by most researchers (Molnar et al., 1989) and industrial practitioners.

Void formation due to other processing parameters

The effects of other processing or material parameters on void formation were also investigated. Figure 10 shows the effect of the liquid-invading velocity on void formation for

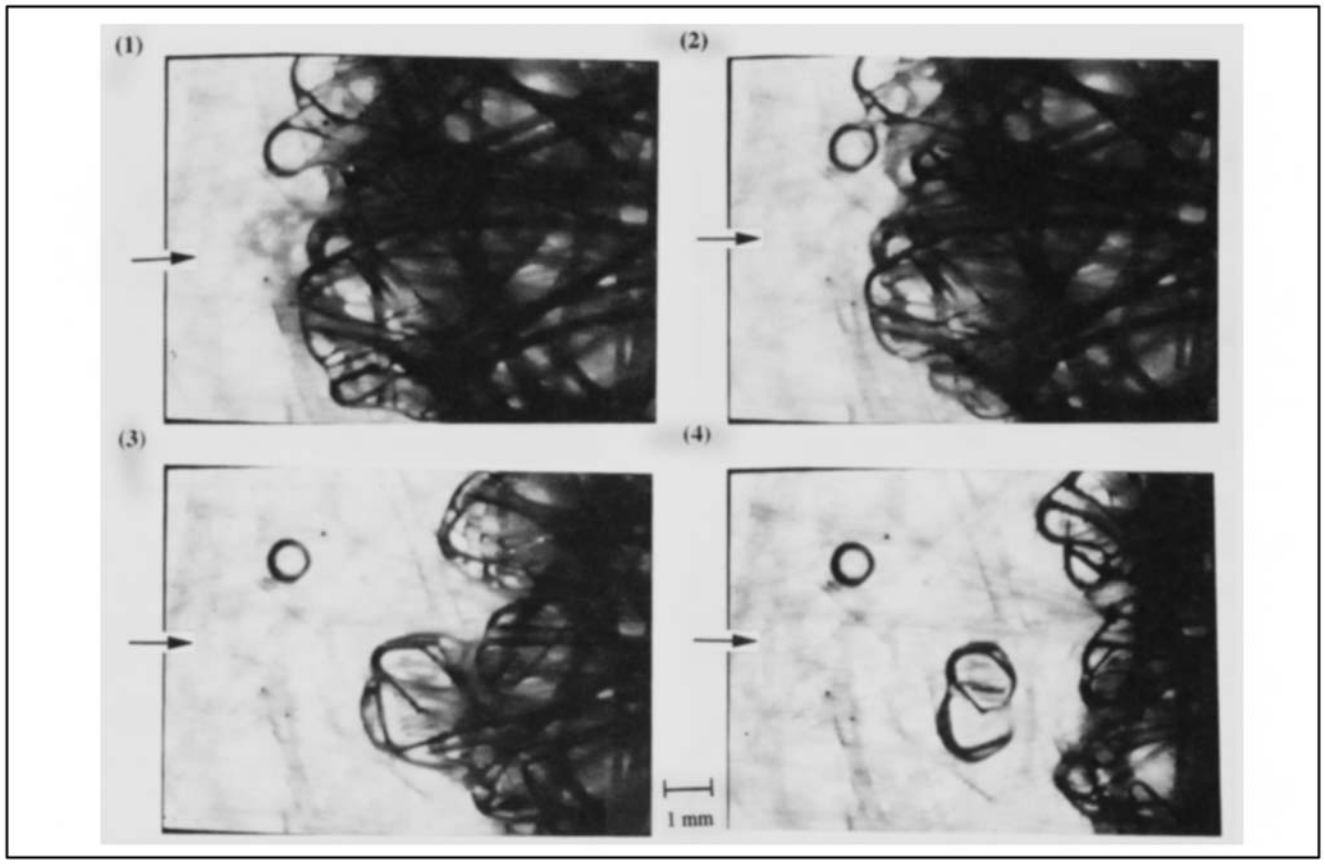

Figure 8. Transient flow front through random fiber mat, velocity = 0.078 cm/s, porosity = 0.89.
(1) 4.36 s; (2) 4.85 s; (3) 8.34 s; (4) 9.2 s.

continuous random fiber mats. Large spherical voids formed at a very slow filling velocity. Cylindrical voids inside fiber bundles increased with increasing flow rates due to the higher degree of liquid bypassing. The void content data were measured after the liquid passed the fiber mats for a relatively long time. In this case, a steady state was reached. If the filling process was stopped after the liquid reached the end of the fiber mats, the quantities of spherical bubbles increased at higher filling rates. This was due to dynamic air bubble mobilization.

The effects of surfactants on void formation in RTM/SRIM processes are not yet available in the literature. The preliminary experimental results from video-enhanced microscopy showed that the surfactants did not reduce voids at a higher filling rate due to the high degree of bypassing. In the case of very slow filling, surfactants did reduce void contents due to the reduction of wetting contact angle. Surface tension plays an important role in two ways for fiber wetting: liquid bypassing/initial air trapping and mobilization. Higher surface tension is favorable in the initial penetration stage, while lower surface tension is favorable in terms of mobilization. The liquid with a higher surface tension can penetrate faster initially. With lower surface tension, the entrapped air voids are more deformable and hence can be washed out of the fiber bundles more efficiently.

Depending on the time scale for mobilization, there is an optimum surface tension for reducing air entrapment. For a low fiber loading system, mobilization is not important and so reducing surface tension will increase the amounts of air entrapped initially. For a highly filled composite process such as RTM, low surface tension is desirable for reducing air bubbles. The same consideration can be applied to the case of mold-filling rate. For higher flow rate processes such as SRIM, lower surface tension is favorable due to the strong mobilization effect. In the case of slow filling-rate processes such as RTM, higher surface tension is favorable due to the importance of initial penetration.

We also examined the effect of viscosity on void formation. Low viscosity is favorable in terms of reducing the amount of air entrapped in the initial trapping stage, while higher viscosity increases the compressing pressure and helps in mobilization. To have good wetting, it is important that the viscosity be no more than a few hundred mPa·s at some stage in the contact process. If the viscosity is too high, the resins penetrate too slowly into the small interstices between fiber filaments. It was also observed during our molding experiment that in the case of extremely low viscosity and fast filling, large amounts of spherical voids formed. This was because turbulent flow occurred when the resin encountered the fiber. Wakes or cavitation caused void formation behind fiber bundles in this case. Figure 11 compares the void images from two different viscosity liquids at a similar filling rate (0.8 cm/s). Figure 11a shows immersion oil (viscosity of 51.5 mPa·s) and Figure 11b shows epoxy resin (viscosity of 650 mPa·s). In the case of epoxy resin, more cylindrical voids were trapped due to its slower penetration into fiber bundles.

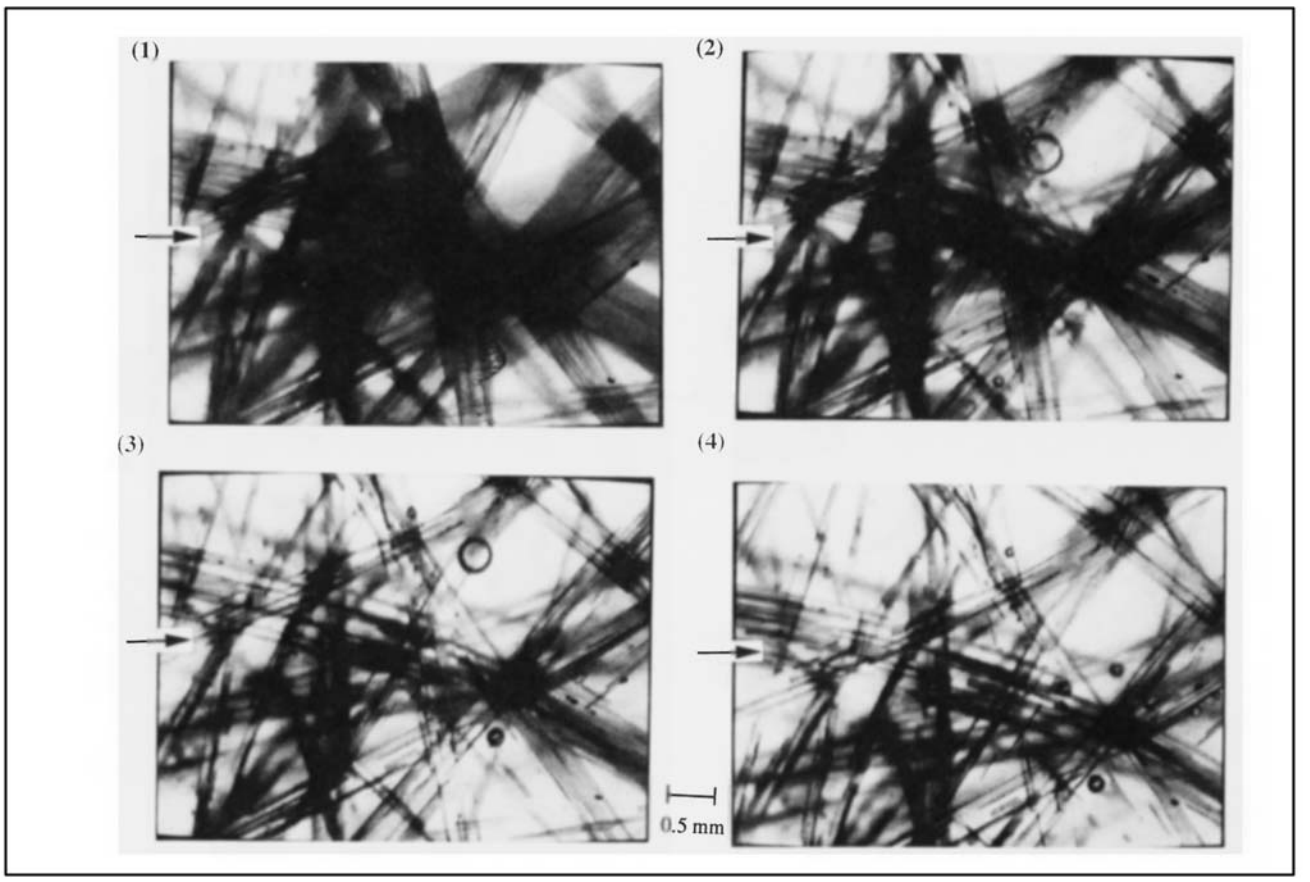

Figure 9. Transient flow front through random fiber mat, velocity = 1.5 cm/s, porosity = 0.89.
(1) 0.07 s; (2) 0.18 s; (3) 0.23 s; (4) 0.3 s.

The effect of temperature mainly reflects on the viscosity and surface tension of resins. Higher temperatures will reduce viscosity and surface tension for most polymers. Since the effect of temperature on reducing viscosity is orders of magnitude greater than that of reducing surface tension, it is easier to achieve better fiber wetting by reducing viscosity. Viscosity can be reduced either by raising the mold temperature or blending the resins with lower molecular weight monomers.

Figures 12a and 12b illustrate the effect of vacuum on void formation with three layers of fiber mats (80% vacuum). It is clearly shown that vacuum dramatically reduced the quantity of voids. In all cases, vacuum dramatically reduced the amount of air entrapped. Hence, vacuum should be the first method used in reducing air entrapment in composite manufacturing. Comparing the void images of one layer with those of three layers, we found that no meso voids existed in the three-layer case. Instead, there were numerous micro voids formed. In all our experiments with high contents of glass fibers, none of the meso voids were observed. In this case, the fiber mats were more compact and the mold pressures were much higher.

Void Content Measurement

The amount of air trapped during flow visualization was quantified by an image-analysis method. Hard copies of flow videos were made using a 35-mm camera or a video hard-copy printer. These images were then integrated by an image analyzer that counted the bubble areas. Digital image analysis was carried out by first scanning the pictures with an Adobe Photoshop Scanner (UMAC UC300), and then analyzing the images with a Macintosh image-analysis program (ULTIMAGE) on digitized binary images.

Digital image analysis can provide more reliable integration, but a note of precaution must be made in order to obtain consistent results. The focusing depth of the microscopic camera was narrow enough such that the image taken technically represented one layer of the fiber mat (about 200 μm). The voids from other fiber layers showed a much lighter image (lower gray level) than those in the focal plain. The analyzer can divide the images into 255 different gray levels. Certain ranges of gray levels were selected to represent the voids. The digitized images were then compared to the original flow picture until they satisfactorily matched. The number of voids was then determined by "threshold" operation in the image-analysis program. Some of the void images required manual pretreatment to make them more accessible for image processing.

The error bar from image analysis is about 1%, including the human factor. This value was obtained by repeating the image analysis several times and by different people. In order to obtain representative void contents for each experiment, three or six pictures were taken from each experiment for image analysis. The void contents were taken as the average value of these three or six measurements. The area fraction

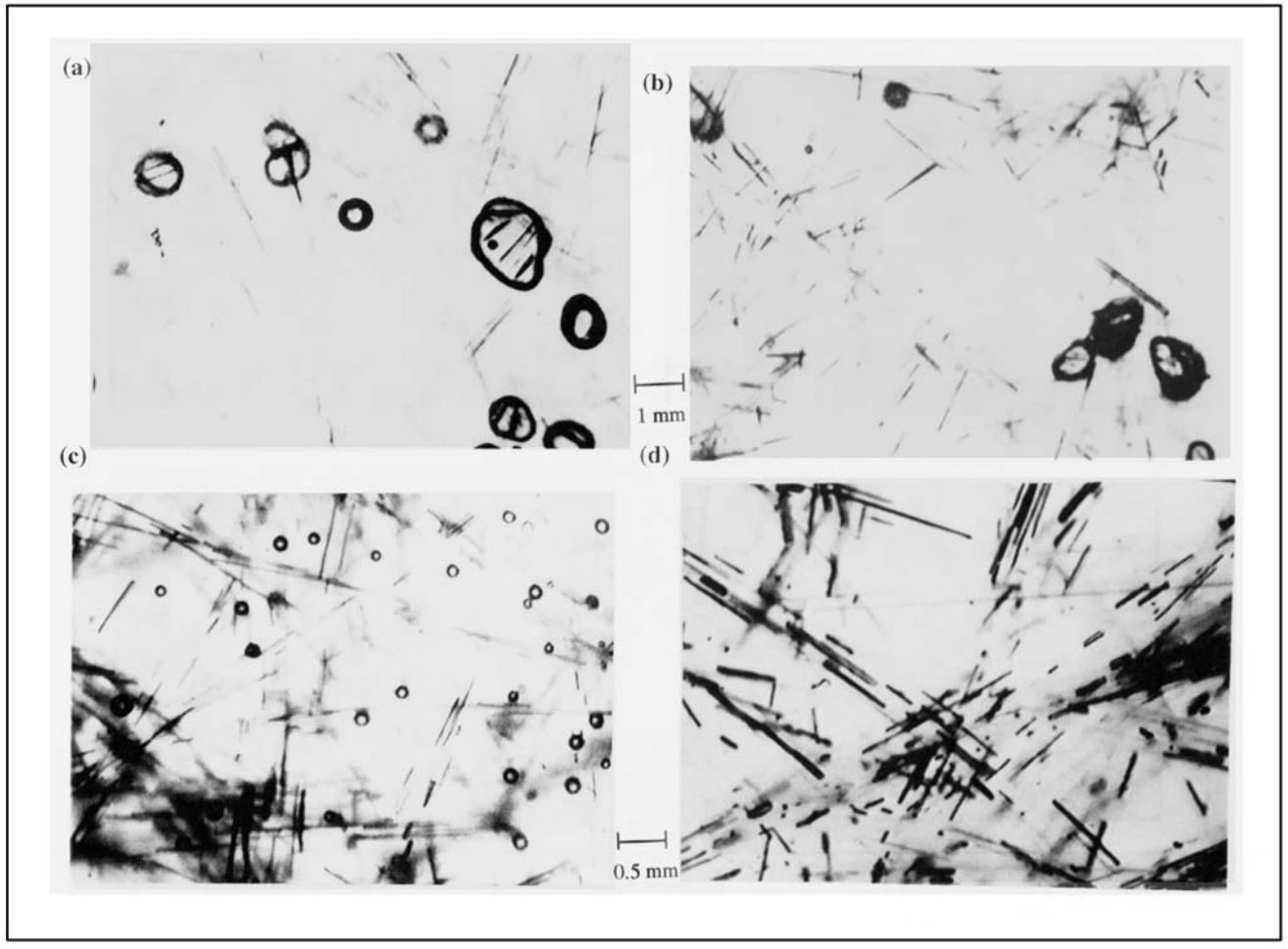

Figure 10. Effects of flow rate on void formations in continuous random fiber mats.

(a) $v = 0.026$ cm.s (11.25×). (b) $v = 0.078$ cm/s (11.25×). (c) $v = 0.175$ cm/s (22.5×). (d) $v = 1.81$ cm/s (22.5×).

cal voids as a function of dimensionless velocity is shown in Figure 13 for both the steady-state and dynamic cases. The dimensionless velocity is taken as the ratio of measured liquid-invading velocity to measured capillary velocity (Eq. 4, Part II). The capillary velocity was estimated from the flow image and confirmed by Eq. 3, Part II. The void contents are taken as the area fraction of voids to the whole image. The results indicated that the quantities of spherical voids decreased with increasing velocity at a steady-state case. The higher void contents below capillary velocity of the immersion oil inside the fiber bundles are mainly due to the joining of the capillary flow fronts.

The void area fraction vs. the dimensionless velocity is shown in Figure 14 for voids of cylindrical shape (micro voids) that were inside the fiber bundles. The fraction of such voids increased with increasing velocity. For the slow filling case, the quantities of micro voids were small and difficult to distinguish between small differences of flow rates. For higher flow rates, the quantities of micro voids increased with increasing flow rates and seemed to level off for a large range and then slightly decrease due to the mobilization mechanism. This is because of the dominance of the liquid bypassing and a weak mobilization effect.

If the flow rate were to keep increasing, the number of micro voids would decrease due to the mobilization effect. Because of the equipment limitation in the laboratory, our flow rates did not go beyond 10 cm/s. An additional limitation is that in order to have a good visualization image, only a few layers of fibers mats can be used. This resulted in a relatively higher porosity compared to the industrial resin transfer molding process. The pressure gradient was simply not high enough to mobilize the voids inside fiber bundles.

Different liquid viscosities and surface tensions were also investigated. Viscosity and surface tension data of the three tested liquids are listed in Table 2. The number of spherical voids as a function of capillary number is shown in Figure 15 for these three liquids. The capillary number is the value of main flow velocity times the fluid viscosity divided by the surface tension of the fluid. The number of spherical voids decreased with increasing velocity at a steady-state case. The void content–capillary number relationship of cylindrical voids is shown in Figure 16. The number of micro voids entrapped increased with increasing velocity. These experiments indicated that the effect of liquid properties such as surface tension and viscosity on void formation can be scaled by capillary number.

It is important to realize that in order to have a fast imbibition speed, a higher surface tension is favorable for the ini-

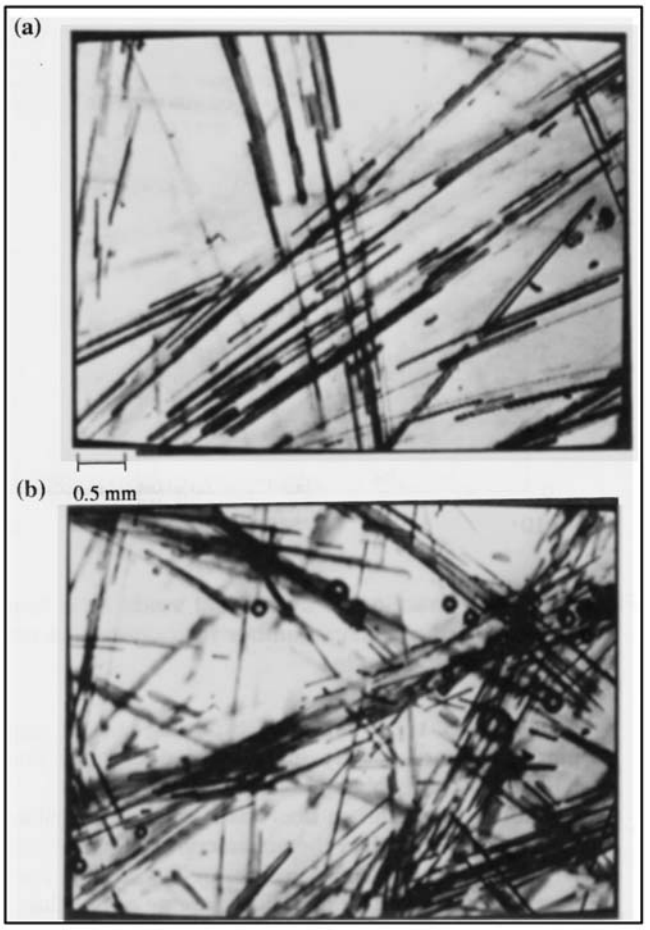

Figure 11. Comparison of void images with different viscosity liquids.

(a) Immersion oil (51.5 cp). (b) Epoxy resin (650) cp). (Filling velocity is 0.8 cm/s.)

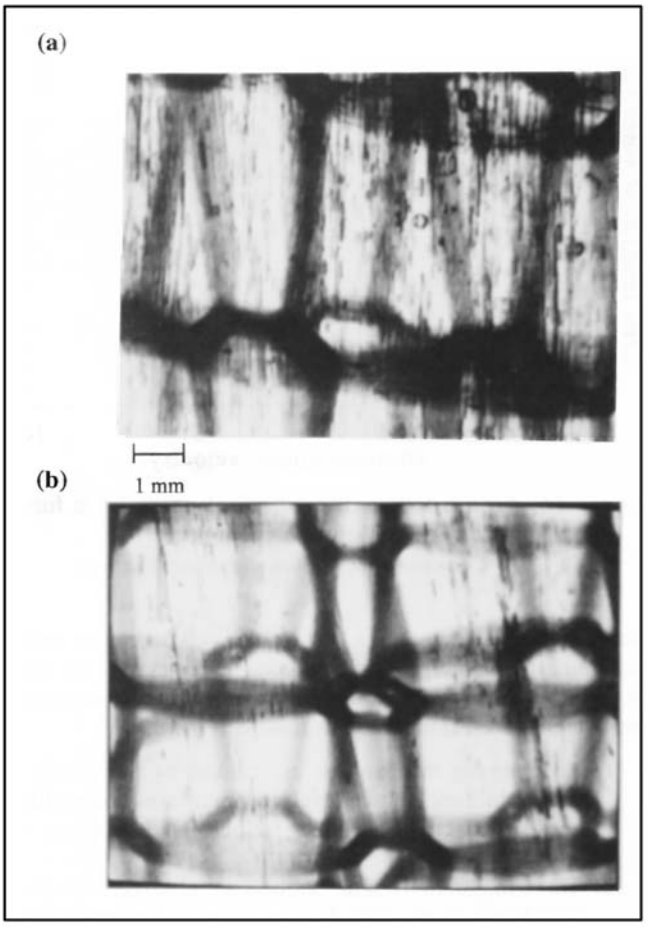

Figure 12. Effect of vacuum on void formation; three layers of fiber mats, porosity = 0.625.

(a) ΔP = 20 psi, without vacuum (11.10×). (b) ΔP = 10 psi, with vacuum (11.10×).

tial liquid penetration. But higher surface tension will increase the pressure gradient necessary for mobilization. The available time for mobilization is also important. It was observed that the number of micro voids entrapped were lower closest to the mold inlet due to a higher degree of mobilization.

The results of the void content–velocity relationship of unidirectional fiber mats are plotted in Figure 17. Both case studies show increasing void content with increasing flow rate. For the transverse fiber direction the amount of air entrapped is higher than that of parallel fiber direction at high flow rates. This can be explained by recognizing that it is more difficult to mobilize voids in the transverse fiber direction due to the smaller pore throat size (the gaps between parallel fibers). Microvoids can eventually move parallel to the fiber bundle until they find a large throat (large gap) through which to escape.

Conclusions

Fiber wetting and void formation of liquid through fiber prepacked molds have been visualized using a refractive in-

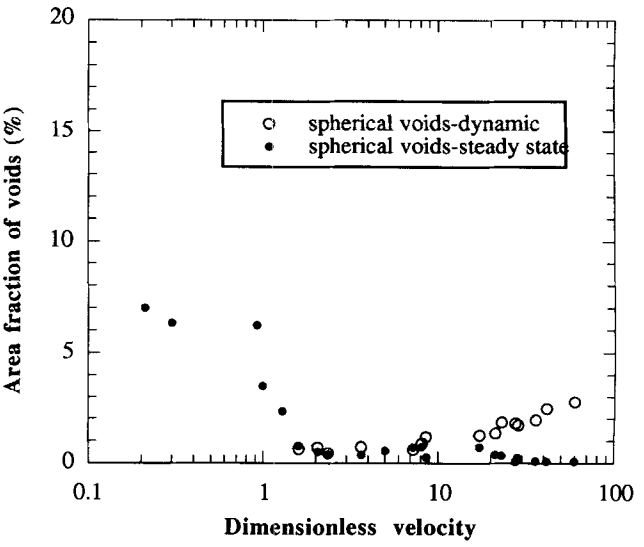

Figure 13. Area fraction of spherical voids as a function of dimensionless velocity.

Pure immersion oil, continuous random fiber mats.

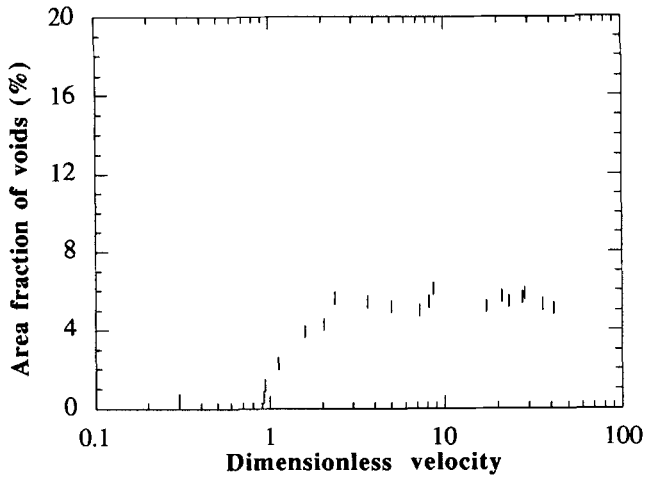

Figure 14. Area fraction of cylindrical voids as a function of dimensionless velocity.

Pure immersion oil, continuous random fiber mats.

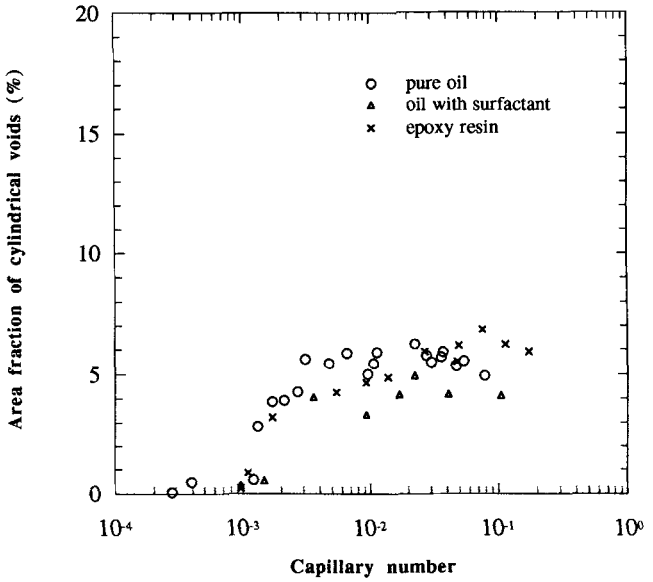

Figure 16. Area fraction of cylindrical voids as a function of capillary number for continuous random fiber mats.

dex matching technique in a rectangular polycarbonate mold. Continuous random and unidirectional fiber mats were used in this study. The major results from our wetting visualization experiments are summarized as follows:

(1) Air trapping mechanisms are caused by two levels of permeabilities: bundle-level and mat-level competition between macroscopic filling velocity and capillary velocity.

(2) Three major kinds of air bubbles are observed: (a) small cylindrical micro voids between fiber filaments (inside fiber bundles); (b) meso voids that encompass many fibers inside the voids (inside fiber bundles); (c) spherical macro voids outside fiber bundles.

(3) Air trapping mechanisms can be described by three major events: (a) initial liquid bypassing and air trapping; (b) later capillary invasion of disordered fiber bundles; (c) air bubble mobilization.

(4) For continuous random fiber mats, when the capillary velocity is greater than the macroscopic filling velocity, large voids are entrapped by the joining of flow fronts along fiber bundles. In the other extreme of fast filling, cylindrical micro voids are entrapped inside fiber bundles due to the bypassing of liquids outside fiber bundles.

(5) Micro voids that are formed randomly due to irregular fiber packing can be mobilized or forced out of fiber bundles when the viscous force is greater than the cap-

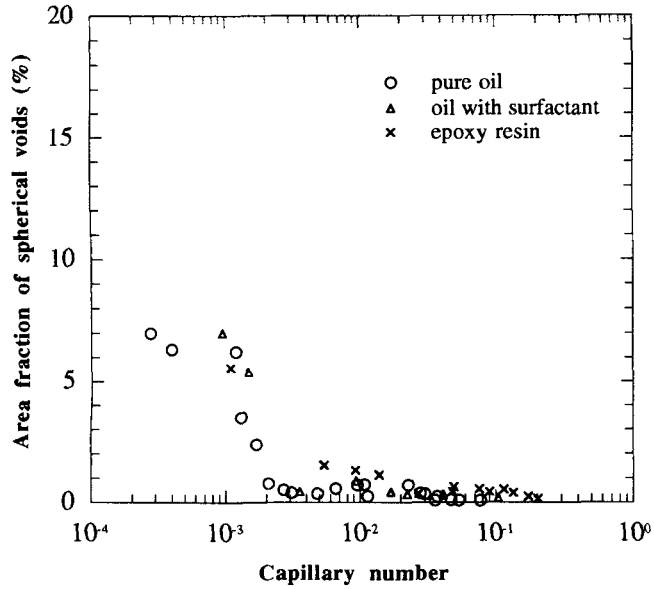

Figure 15. Area fraction of spherical voids as a function of capillary number for continuous random fiber mats.

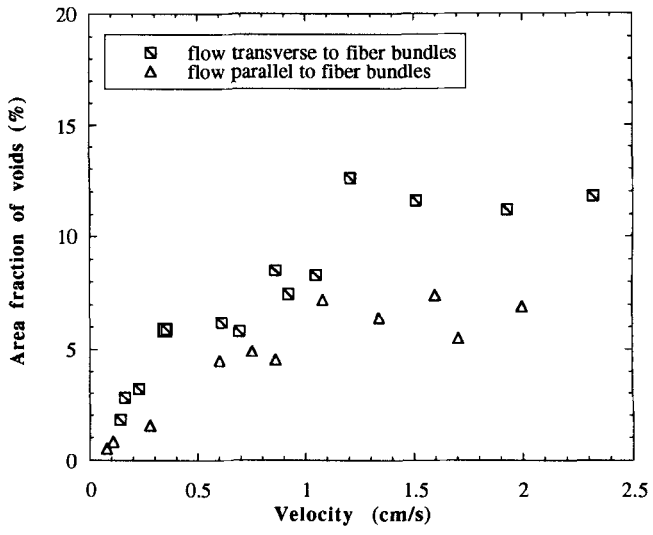

Figure 17. Area fraction of voids inside large fiber bundle as a function of velocity.

Test liquid is immersion oil.

illary force holding them in place. When forced out of the fiber bundles, these small voids become spherical in shape.

(6) The number of spherical bubbles decrease in number density with increasing flow rate at a steady state, but accumulate at the end of the mold; the number of cylindrical voids increase in number density with increasing flow rate, and are less dependent on the mold position.

What we have learned from the wetting visualization enables one to formulate better guidelines for optimum processing parameters of fiber wetting for resin transfer molding (RTM) and structural reaction injection molding (SRIM). These are that low viscosity, high mold temperature, and high pressure should be used whenever possible. A vacuum should be applied if possible. Increasing fiber loading (fiber content) will reduce the quantities of voids entrapped. If capillarity is dominant, surfactants can help in reducing voids by reducing the wetting contact angle. But for the usual production speed, the use of surfactants is questionable unless it is for a very high fiber loading application.

Acknowledgments

The authors would like to thank the Center of Interfacial Engineering at the University of Minnesota, Rhone-Poulenc Inc., and Moldflow Ltd. for the financial support provided for this research. The authors would also like to thank Wieslaw Suszynski, Jason Chou and Mark Tapsak for their help on part of the visualization experiments.

Literature Cited

Bascom, W. D., and J. B. Romans, "Micro Voids in Glass-Resin Composite," *Ind. Eng. Chem. Prod. Res. Dev.*, **7**, 172 (1968).

Behrens, R. A., Tech. Rep. No. CCM-83-14, Center for Composite Materials, Univ. of Delaware, Newark (1983).

Chan, A. W., and R. J. Morgan, "Modeling Preform Impregnation and Void Formation in Resin Transfer Molding of Unidirectional Composites," *SAMPE Q.*, 48, (Apr. 1992).

Chen, Y. T., H. T. Davis, and C. W. Macosko, "Wetting of Fiber Mats for Composites Manufacturing: II. Air Entrapment Model," *AIChE J.*, **41**, 2274 (1995).

Chen, Y. T., "Resin Transfer Molding of Polycyanate: Chemorheology, Molding Experiment, and Wetting Visualization," PhD Diss., Univ. of Minnesota, Minneapolis (1993).

Elmendorp, J. J., and F. During, "Dynamic Wetting Aspects of Melt Impregnation of Fiber Mats," *ANTEC*, 1361 (1990).

Gonzalez, V. M., "Studies of Reactive Polymer Processing with Fiberglass Reinforcement," PhD Diss., Univ. of Minnesota, Minneapolis (1983).

Gutowski, T. G., Z. Cai, S. Bauer, J. Boucher, J. Kingery, and S. Wineman, "Consolidation Experiment for Laminate Composites," *J. Compos. Mat.*, **21**, 650 (1987).

Hayward, J. S., and B. Harris, "The Effect of Vacuum Assistance in Resin Transfer Molding," *Compos. Manuf.*, **1**, 161 (1990).

Judd, N. C. W., and W. W. Wright, "Voids and Their Effects on the Mechanical Properties of Composites—An Appraisal," *SAMPE J.*, **14**, 10 (1978).

Kamal, M. R., P. Singh, Q. Samak, and S. M. Kakarala, "Microstructure and Mechanical Behavior of Reinforced Reaction Injection Molded (RRIM) Polyurethane," *ANTEC*, 1362 (1986).

Kardos, M. P., A. Dudukovic, and R. Dave, *Advances in Polymer Science: Epoxy Resin and Composite*, K. Dusek, ed., Springer-Verlag, New York, p. 101 (1986).

Kohn, E. J., A. G. Sands, and R. C. Clark, "Quantitative Measurement of Void Content in Glass-Filament-Wound Composites and Correlation of Interlaminar Shear Strength with Void Content," *Ind. Eng. Chem. Prod. Res. Dev.*, **7**, 179 (1968).

Lundstrom, T. S., B. R. Gebart, and C. Y. Lundemo, "Void Formation in RTM," *Proc. Conf. Composites Institute, SPI*, Session 16-F (1992).

Macosko, C. W, "Fundamentals of Reaction Injection Molding," Hanser, New York, p. 209 (1989).

Mahale, A. D., R. K. Prud'homme, and L. Rebenfeld, "Quantitative Measurement of Voids Formed During Liquid Impregnation of Nonwoven Multifilament Glass Networks Using an Optical Visualization Technique," *Poly. Eng. Sci.*, **32**, 319 (1992).

McGeehan, J. A., "Processing/Performance Relationships Considering Voids in Structural Reaction Injection Molded Composites," Tech. Rep. No. CCM-91-21, Center for Composite Materials, Univ. of Delaware, Newark (1991).

Molnar, J. A., L. Trevino, and L. J. Lee, "Liquid Flow in Molds with Prelocated Fiber Mats," *Polym. Compos.*, **10**, 414 (1989).

Parnas, R. S., and F. R. Phelan, Jr., "The Effect of Heterogeneous Porous Media on Mold Filing in Resin Transfer Molding," *SAMPE Q.*, 53 (Jan., 1991).

Stabler, W. R., G. B. Tatterson, R. L. Sadler, and A. H. M. El-Shiekh, "Void Minimization in the Manufacturing of Carbon Fiber Composites by Resin Transfer Molding," *SAMPE Q.*, 38 (Jan., 1992).

Williams, J. G., C. E. Morris, and B. C. Ennis, "Liquid Flow Through Aligned Fiber Beds," *Poly. Eng. Sci.*, **14**, 413 (1974).

Manuscript received Sept. 22, 1993, and revision received Nov. 23, 1994.